Geomechanics and Engineering, *Vol. 35, No. 1 (2023) 81-93*
https://doi.org/10.12989/gae.2023.35.1.081

The effects of temperature and porosity on resonance behavior of graphene platelet reinforced metal foams doubly-curved shells with geometric imperfection

Jiaqin Xu and Gui-Lin She*

College of Mechanical and Vehicle Engineering, Chongqing University, Chongqing 400044, China

(*Received January 31, 2023, Revised August 28, 2023, Accepted September 4, 2023*)

Abstract. Due to the unclear mechanism of the influence of temperature on the resonance problem of doubly curved shells, this article aims to explore this issue. When the ambient temperature rises, the composite structure will expand. If the thermal effects are considered, the resonance response will become more complex. In the design of structure, thermal effect is inevitable. Therefore, it is of significance to study the resonant behavior of doubly curved shell structures in thermal environment. In view of this, this paper extends the previous work (She and Ding 2023) to the case of the nonlinear principal resonance behavior of graphene platelet reinforced metal foams (GPLRMFs) doubly curved shells in thermal environment. The effect of uniform temperature field is taken into consideration in the constitutive equation, and the nonlinear motion control equation considering temperature effect is derived. The modified Lindstedt Poincare (MLP) method is used to obtain the resonance response of doubly curved shells. Finally, we study the effects of temperature changes, shell types, material parameters, initial geometric imperfection and prestress on the forced vibration behaviors. It can be found that, as the temperature goes up, the resonance position can be advanced.

Keywords: doubly curved shells; geometric imperfection; graphene platelet reinforced metal foams; resonance; thermal effects

1. Introduction

The research on the vibration behavior of structures in thermal environment has very important engineering background and theoretical value (Abdelrahman *et al.* 2022, Alazwari *et al.* 2021, Ahmed *et al.* 2021, Basha *et al.* 2022, Emadi *et al.* 2021, Babaei 2022a, b, Babaei and Eslami 2021a, b, Chen *et al.* 2022a, b, Ding *et al.* 2023, Ding and She 2021, Ding *et al.* 2022a, Li *et al.* 2023, She *et al.* 2021, She and Li 2022, Wu and She 2023, Xu and She 2022, 2023, Zhang *et al.* 2022, Zhang *et al.* 2023c, Zhang and She 2022, 2023b, Zhao *et al.* 2022a, Hong *et al.* 2020, 2021, Duc *et al.* 2018, Chan *et al.* 2019). Many scholars studied the vibration response and resonance behavior of plate and shell structures in thermal environment (Ahmadi *et al.* 2019, Foroutan *et al.* 2021, Aris *et al.* 2022, Li *et al.* 2022, 2021, Ahmadi *et al.* 2020, Shi *et al.* 2021, Tu *et al.* 2021, Ding *et al.* 2023c). For example, studied the nonlinear vibration behavior of energy gradient cylindrical shells in thermal environment using multi-scale method. Ahmadi *et al.* (2021) employed Galerkin method to study the nonlinear thermal buckling of FG spherical shells under thermal environment. Safarpour *et al.* (2019) established the governing equations of composite cylindrical shells by Hamiltonian principle, and studied their thermal buckling and vibration characteristics. Dastjerdi *et al.* (2020) studied the nonlinear dynamic analysis of cylindrical shells considering the hydrothermal environment based on the first-order shear theory. Ebrahimi *et al.* (2020) used the improved coupled stress theory to analyze the thermal buckling and forced vibration characteristics of graphene reinforced cylindrical shell. Li *et al.* (2022) studied the free vibration of composite conical shells under thermal environment by Galerkin method. Hajilak *et al.* (2019) premeditated the forced vibration and buckling behavior of graphene reinforced cylindrical shells in thermal environment based on the modified strain gradient theory. Chan *et al.* (2019) studied the dynamics of FG shells in thermal environment based on the CSTY with geometric nonlinearity. Abuteir *et al.* (2021) intended the dynamic buckling behavior of FG material shells structures in thermal environment. Nguyen *et al.* (2019) studied the nonlinear vibration response of carbon nanotube reinforced shells in thermal environment. Rout *et al.* (2019) used the finite element method to study the free vibration response of carbon nanotube reinforced cylindrical shells in the thermal environment. Liu *et al.* (2019) calculated the natural frequency of FG shells in thermal environment based on Donnell's shell theory. Zu *et al.* (2022) used Rayleigh Ritz method to study the vibration characteristics of graphene cylindrical shells in thermal environment. Shakouri *et al.* (2019) studied the vibration behavior of FG conical shells at high temperatures using Donnell shell theory. Duc *et al.* (2019) studied the vibration and nonlinear dynamic response of FG cylindrical plates in thermal environment. Rout *et al.* (2021) studied the free vibration

*Corresponding author, Associate Professor
E-mail: sheguilin@cqu.edu.cn

ISSN: 2005-307X (Print), 2092-6219 (Online)

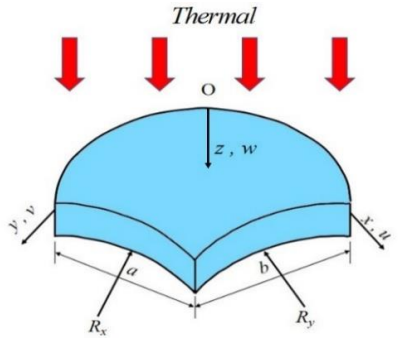

Fig.1 The shell

characteristics of FG conical shells under thermal load based on the first-order shear theory. Heydarpour *et al.* (2020) analyzed the dynamic response of FG graphene reinforced cylindrical shells under impact loading by differential integration. Maji *et al.* (2020) discussed the free vibration characteristics of carbon nanotube reinforced shells considering rotational motion and temperature based on the first-order shear theory. Abuteir *et al.* (2022) researched the free vibration response of FG cylindrical shells under thermal environment using the principle of virtual work. Baghlani *et al.* (2020) analyzed the free vibration of FG cylindrical shells in thermal environment based on CSTY. Dat *et al.* (2020) studied the nonlinear dynamic response of carbon nanotube reinforced cylindrical shell in thermal environment based on the CSTY with von Karman geometric nonlinearity. Karimiasl *et al.* (2019) researched the thermal post buckling characteristics of composite shells under thermal environment. Fu *et al.* (2020) studied the dynamic behavior of FG cylindrical shells in thermal environment based on Hamilton principle. Chen *et al.* (2022) explored the thermal post-buckling behavior of sandwich cylindrical shells under thermal environment. Wang *et al.* (2021) analyzed the dynamic characteristics of spherical shells under thermal environment. More works can refer to Refs. (Daikh *et al.* 2021, Emam *et al.* 2018, Esen *et al.* 2022, Hendi *et al.* 2022, Mohamed *et al.* 2019, 2021, Melaibari *et al.* 2023).

However, there is no research on nonlinear resonance of GPLRMFs doubly curved shells in thermal environment. In this paper, considering the uniform temperature changes, the nonlinear motion equations incorporating temperature effect are deduced. The MLP method is employed to obtain the resonance response of doubly curved shells. Finally, the effects of various factors on the forced vibration behaviors are discussed in detail.

2. Material properties

In this paper, we consider four types of doubly-curved shells, namely, cylindric shell (R_x=R, R_y=→∞), hyperbolic shell (R_x=R, R_y=−R), spherical shell (R_x=R, R_y=R), and elliptical shell (R_x=R, R_y=2R). The length, width, and thickness of the shell are respectively represented by a, b, and h, as shown in Figs. 1 and 2. Also, we consider the properties of materials to vary in the form of functional gradients (Ding *et al.* 2022b, Lu *et al.* 2021, She *et al.* 2021, 2022, Xu *et al.* 2023, Zhang *et al.* 2023a, d, Zhang *et al.* 2021, Zhao *et al.* 2022b, Ding *et al.* 2023), in which three different types of porosity distribution, of which the first and second (including Porosity-I and Porosity-II) are the cosine functions of thickness z, and the third (Porosity-III) is uniform and independent of thickness z, with the specific expressions (Kitipornchai *et al.* 2017)

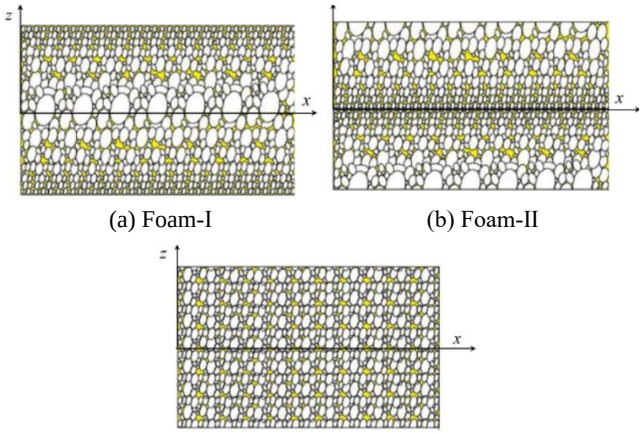

(a) Foam-I (b) Foam-II

(c) Foam-III

Fig. 2 Material characteristics (Wang and Wu 2017)

$$E(z,T)=\begin{cases}E^{\#}\left[1-\mathrm{e}_1\cos(\pi z/h)\right], & (\text{Porosity-I})\\ E^{\#}\left\{1-\mathrm{e}_2\left[1-\cos(\pi z/h)\right]\right\}, & (\text{Porosity-II})\\ E^{\#}\mathrm{e}_3, & (\text{Porosity-III})\end{cases}$$
$$\rho(z,T)=\begin{cases}\rho^{\#}\left[1-\mathrm{e}_{m1}\cos(\pi z/h)\right], & (\text{Porosity-I})\\ \rho^{\#}\left\{1-\mathrm{e}_{m2}\left[1-\cos(\pi z/h)\right]\right\}, & (\text{Porosity-II})\\ \rho^{\#}\mathrm{e}_{m3}, & (\text{Porosity-III})\end{cases} \quad (1)$$
$$\alpha(z)=\alpha^{\#},\mu(z)=\mu^{\#}$$

Herein, the material properties of the doubly curved shells without pores are denoted by $E^{\#}$, $\rho^{\#}$, $\alpha^{\#}$, $\mu^{\#}$. e_i, $\mathrm{e}_{mi}(i=1,2,3)$ is used for porosity coefficient, which can be described as (Kitipornchai *et al.* 2017, Ding and She 2023a, Gan and She 2023, Gan *et al.* 2023, She and Ding 2023, Song and She 2023, Zhang *et al.* 2023b, Zhang and She 2023a)

$$E^{\#}=\frac{3}{8}\left\{\frac{1+\zeta_L V_{GPL}\left[\frac{(E_{GPL}/E_M)-1}{(E_{GPL}/E_M)+2(l_{GPL}/h_{GPL})}\right]}{1-\left[\frac{(E_{GPL}/E_M)-1}{(E_{GPL}/E_M)+2(l_{GPL}/h_{GPL})}\right]V_{GPL}}\right\}\times E_M$$
$$+\frac{5}{8}\left\{\frac{1+\zeta_W V_{GPL}\left[\frac{(E_{GPL}/E_M)-1}{(E_{GPL}/E_M)+2(l_{GPL}/h_{GPL})}\right]}{1-\left[\frac{(E_{GPL}/E_M)-1}{(E_{GPL}/E_M)+2(l_{GPL}/h_{GPL})}\right]V_{GPL}}\right\}\times E_M \quad (2)$$

$$\begin{bmatrix}\rho^{\#}\\ \alpha^{\#}\\ \mu^{\#}\end{bmatrix}=V_{GPL}\begin{bmatrix}\rho_{GPL}\\ \alpha_{GPL}\\ \mu_{GPL}\end{bmatrix}+(1-V_{GPL})\begin{bmatrix}\rho_M\\ \alpha_M\\ \mu_M\end{bmatrix} \quad (3)$$

in which, the subscript M is used for matrix material, GPL for graphene platelet, V_{GPL} is the GPLs volume fraction, in addition

$$\frac{E(z,T)}{E_c}=\left[\frac{\rho(z)}{\rho_c}\right]^2 \tag{4}$$

$$\begin{cases}1-e_{\mathrm{m}1}\cos(\pi z/h)=\sqrt{1-e_1\cos(\pi z/h)}\\ 1-e_{\mathrm{m}2}\left[1-\cos(\pi z/h)\right]=\sqrt{1-e_2\left[1-\cos(\pi z/h)\right]}\\ e_{\mathrm{m}3}=\sqrt{e_3}\end{cases} \tag{5}$$

Additionally, because the total masses of matrix for Porosity-I, Porosity-II and Porosity-III are equal, we have

$$\int_0^{\frac{h}{2}}\sqrt{1-e_1\cos(\pi z/h)}dz=\int_0^{\frac{h}{2}}\sqrt{e_3}dz=\int_0^{\frac{h}{2}}\sqrt{1-e_2\left[1-\cos(\pi z/h)\right]}dz \tag{6}$$

Three GPLs reinforced types (including GPL-A, GPL-B and GPL-C) are taken into account, in addition

$$V_{TGPL}\int_{-h/2}^{h/2}\frac{\rho(z)}{\rho^{\#}}\mathrm{d}z=\begin{cases}\int_{-h/2}^{h/2}Si_1\left[1-\cos(\pi z/h)\right]\frac{\rho(z)}{\rho^{\#}}\mathrm{d}z, & (\text{GPL-A})\\ \int_{-h/2}^{h/2}Si_2\cos(\pi z/h)\frac{\rho(z)}{\rho^{\#}}\mathrm{d}z, & (\text{GPL-B})\\ \int_{-h/2}^{h/2}Si_3\frac{\rho(z)}{\rho^{\#}}\mathrm{d}z, & (\text{GPL-C})\end{cases} \tag{7}$$

The total GPLs volume fraction V_{TGPL} have the following expression (Chai and Wang 2022, Wang *et al*. 2019)

$$V_{TGPL}=\frac{W_{gpl}}{W_{gpl}+(\rho_{gpl}+\rho_m)(1-W_{gpl})} \tag{8}$$

where, W_{gpl} refers to the GPLs weight fraction.

3. Governing equations

In this paper, we use the Reddy' shell model to describe the displacement field for the doubly curved shells, which considers the shear deformation without introducing the shear factor (She and Ding 2023).

$$\begin{aligned}&u=u_0-z\varphi_x-c_1z^3(\varphi_x+\frac{\partial w_0}{\partial x}),v=v_0-z\varphi_y\\&-c_1z^3(\varphi_y+\frac{\partial w_0}{\partial y}),w=w_0+w_1.\end{aligned} \tag{9}$$

in Eq. (9), $c_1=\frac{4}{3h^2}$, $c_2=3c_1$. The strains of interest $\varepsilon_x,\varepsilon_y,\gamma_{xy},\gamma_{xz},\gamma_{yz}$ have the same expression as our previous work (She and Ding 2023). The constitutive equation considering thermal effect has the following expression

$$\begin{bmatrix}\sigma_x\\ \sigma_y\\ \sigma_{xz}\\ \sigma_{yz}\\ \sigma_{xy}\end{bmatrix}=\begin{bmatrix}Q_{11}&Q_{12}&0&0&0\\ Q_{12}&Q_{22}&0&0&0\\ 0&0&Q_{44}&0&0\\ 0&0&0&Q_{55}&0\\ 0&0&0&0&Q_{66}\end{bmatrix}\begin{bmatrix}\varepsilon_x\\ \varepsilon_y\\ \gamma_{xz}\\ \gamma_{yz}\\ \gamma_{xy}\end{bmatrix}-\alpha(z)\begin{bmatrix}\Delta T\\ \Delta T\\ 0\\ 0\\ 0\end{bmatrix} \tag{10}$$

With ΔT being the uniform temperature changes, and

$$\begin{aligned}&Q_{11}=Q_{22}=\frac{E(z,T)}{1-\left[\mu(z)\right]^2},\ Q_{66}=\frac{E(z,T)}{2(1+\left[\mu(z)\right])},\\&Q_{12}=\frac{vE(z,T)}{1-\left[\mu(z)\right]^2},\ Q_{55}=Q_{44}=Q_{66}.\end{aligned} \tag{11}$$

According to Euler-Lagrange equation, the following equations of motion including thermal effect can be arrived at

$$\begin{aligned}&A_{11}\frac{\partial^2u}{\partial x^2}+A_{66}\frac{\partial^2u}{\partial y^2}+(A_{12}+A_{66})\frac{\partial^2v}{\partial x\partial y}+A_{11}\frac{\partial^2w}{\partial x^2}\frac{\partial w}{\partial x}\\&+A_{66}\left(\frac{\partial^2w_1}{\partial y^2}\frac{\partial w}{\partial x}+\frac{\partial^2w}{\partial y^2}\frac{\partial w_1}{\partial x}+\frac{\partial^2w_1}{\partial x\partial y}\frac{\partial w}{\partial y}+\frac{\partial^2w}{\partial x\partial y}\frac{\partial w_1}{\partial y}\right)\\&+A_{11}\left(\frac{\partial^2w_1}{\partial x^2}\frac{\partial w}{\partial x}+\frac{\partial^2w}{\partial x^2}\frac{\partial w_1}{\partial x}\right)+A_{12}\left(\frac{\partial^2w_1}{\partial x\partial y}\frac{\partial w}{\partial y}\right)\\&+A_{12}\frac{\partial^2w}{\partial x\partial y}\frac{\partial w_1}{\partial y}+A_{12}\frac{\partial^2w}{\partial x\partial y}\frac{\partial w}{\partial y}+A_{66}\left(\frac{\partial^2w}{\partial y^2}\frac{\partial w}{\partial x}\right)\\&+A_{66}\frac{\partial^2w}{\partial x\partial y}\frac{\partial w}{\partial y}+(B_{11}-c_1E_{11})\frac{\partial^2\varphi_x}{\partial x^2}+(B_{66}-c_1E_{66})\frac{\partial^2\varphi_x}{\partial y^2}\\&-\left(\frac{A_{11}}{R_x}+\frac{A_{12}}{R_y}\right)\frac{\partial w}{\partial x}+\left[\begin{matrix}(B_{12}-c_1E_{12})\\ +(B_{66}-c_1E_{66})\end{matrix}\right]\frac{\partial^2\varphi_y}{\partial x\partial y}=\overline{I}_1\frac{\partial^2u}{\partial t^2}\\&+\overline{I}_2\frac{\partial\varphi_x}{\partial t^2}-c_1\overline{I}_3\frac{\partial^3w}{\partial x\partial t^2},\end{aligned} \tag{12}$$

$$\begin{aligned}&(A_{12}+A_{66})\frac{\partial^2u}{\partial x\partial y}+A_{66}\frac{\partial^2v}{\partial x^2}+A_{22}\frac{\partial^2v}{\partial y^2}\\&+A_{66}\left(\frac{\partial^2w_1}{\partial x\partial y}\frac{\partial w}{\partial x}+\frac{\partial^2w}{\partial x\partial y}\frac{\partial w_1}{\partial x}+\frac{\partial^2w_1}{\partial x^2}\frac{\partial w}{\partial y}\right)\\&+A_{66}\frac{\partial^2w}{\partial x^2}\frac{\partial w_1}{\partial y}+A_{12}\left(\frac{\partial^2w_1}{\partial x\partial y}\frac{\partial w}{\partial x}+\frac{\partial^2w}{\partial x\partial y}\frac{\partial w_1}{\partial x}\right)\\&+A_{12}\frac{\partial^2w}{\partial x\partial y}\frac{\partial w}{\partial x}+A_{22}\frac{\partial^2w}{\partial y^2}\frac{\partial w}{\partial y}-\frac{A_{22}}{R_y}\\&+A_{22}\left(\frac{\partial^2w_1}{\partial y^2}\frac{\partial w}{\partial y}+\frac{\partial^2w}{\partial y^2}\frac{\partial w_1}{\partial y}\right)+A_{66}\left(\frac{\partial^2w}{\partial x\partial y}\frac{\partial w}{\partial x}\right)\\&+A_{66}\frac{\partial^2w}{\partial x^2}\frac{\partial w}{\partial y}+(B_{12}-c_1E_{12})\frac{\partial^2\varphi_x}{\partial x\partial y}\\&+(B_{66}-c_1E_{66})\left(\frac{\partial^2\varphi_x}{\partial x\partial y}+\frac{\partial^2\varphi_y}{\partial x^2}\right)-\frac{A_{12}}{R_x}\frac{\partial w}{\partial y}\\&+(B_{22}-c_1E_{22})\frac{\partial^2\varphi_y}{\partial y^2}=\overline{I}_1\frac{\partial^2v}{\partial t^2}+\overline{I}_2\frac{\partial\varphi_y}{\partial t^2}-c_1\overline{I}_3\frac{\partial^3w}{\partial y\partial t^2},\end{aligned} \tag{13}$$

$$\begin{aligned}&c_1\left(E_{11}\frac{\partial^3u}{\partial x^3}+E_{12}\frac{\partial^3u}{\partial x\partial y^2}+2E_{66}\frac{\partial^3u}{\partial x\partial y^2}\right)\\&+\frac{A_{11}}{R_x}\frac{\partial u}{\partial x}+\frac{A_{12}}{R_y}\frac{\partial u}{\partial x}+c_1\left(E_{12}\frac{\partial^3v}{\partial x^2\partial y}+2E_{66}\frac{\partial^3v}{\partial x^2\partial y}\right)\\&+c_1E_{22}\frac{\partial^3v}{\partial y^3}+\left(A_{55}+2c_2D_{55}+c_2^2F_{55}-\frac{c_1E_{11}}{R_x}\right)\frac{\partial^2w}{\partial x^2}\\&-\left(\frac{A_{11}}{R_x^2}+\frac{2A_{12}}{R_xR_y}+\frac{A_{22}}{R_y^2}\right)w+\left(c_2^2F_{44}-\frac{c_1E_{22}}{R_y}\right)\frac{\partial^2w}{\partial y^2}\\&+\frac{\partial^2w}{\partial y^2}(A_{44}+2c_2D_{44})+\frac{A_{22}}{R_y}\frac{\partial w_1}{\partial y}\frac{\partial w}{\partial y}+\frac{A_{12}}{R_x}\frac{\partial w_1}{\partial y}\frac{\partial w}{\partial y}\\&+\frac{A_{11}}{R_x}\frac{\partial w_1}{\partial x}\frac{\partial w}{\partial x}+c_1E_{11}\left(\frac{\partial^3w_1}{\partial x^3}\frac{\partial w}{\partial x}+\frac{\partial^3w}{\partial x^3}\frac{\partial w_1}{\partial x}+2\frac{\partial^2w_1}{\partial x^2}\frac{\partial^2w}{\partial x^2}\right)\\&+c_1E_{22}\left(\frac{\partial^3w_1}{\partial y^3}\frac{\partial w}{\partial y}+\frac{\partial^3w}{\partial y^3}\frac{\partial w_1}{\partial y}+2\frac{\partial^2w_1}{\partial y^2}\frac{\partial^2w}{\partial y^2}\right)+\frac{A_{12}}{R_x}\frac{\partial v}{\partial y}\\&+\frac{A_{22}}{R_y}\frac{\partial v}{\partial y}+\frac{A_{12}}{R_y}\frac{\partial w_1}{\partial x}\frac{\partial w}{\partial x}+c_1E_{12}\left(\frac{\partial^3w_1}{\partial x^2\partial y}\frac{\partial w}{\partial y}+\frac{\partial^3w}{\partial x^2\partial y}\frac{\partial w_1}{\partial y}\right)\\&+c_1E_{12}\left(2\frac{\partial^2w_1}{\partial x\partial y}\frac{\partial^2w}{\partial x\partial y}+\frac{\partial^3w_1}{\partial x\partial y^2}\frac{\partial w}{\partial x}+\frac{\partial^3w}{\partial x\partial y^2}\frac{\partial w_1}{\partial x}+2\frac{\partial^2w_1}{\partial x\partial y}\frac{\partial^2w}{\partial x\partial y}\right)\\&+2c_2E_{66}\left(\frac{\partial^3w_1}{\partial x\partial y^2}\frac{\partial w}{\partial x}+\frac{\partial^3w}{\partial x\partial y^2}\frac{\partial w_1}{\partial x}+\frac{\partial^2w_1}{\partial x^2}\frac{\partial^2w}{\partial y^2}+2\frac{\partial^2w_1}{\partial x\partial y}\frac{\partial^2w}{\partial x\partial y}\right)\\&+2c_2E_{66}\left(\frac{\partial^3w_1}{\partial x^2\partial y}\frac{\partial w}{\partial y}+\frac{\partial^3w}{\partial x^2\partial y}\frac{\partial w_1}{\partial y}+\frac{\partial^2w_1}{\partial y^2}\frac{\partial^2w}{\partial x^2}\right)-N_T\frac{\partial^2w}{\partial x^2}\\&-N_T\frac{\partial^2w}{\partial y^2}+\left(\frac{A_{11}}{2R_x}+\frac{A_{12}}{2R_y}\right)\left[\left(\frac{\partial w}{\partial x}\right)^2+\left(\frac{\partial w}{\partial y}\right)^2\right]\\&-\left(\frac{A_{11}}{R_x}+\frac{A_{12}}{R_y}\right)\left(w\frac{\partial^2w}{\partial x^2}+w\frac{\partial^2w}{\partial y^2}\right)+c_1E_{11}\left(\left(\frac{\partial^2w}{\partial x^2}\right)^2+\frac{\partial^3w}{\partial x^3}\frac{\partial w}{\partial x}\right)\\&+A_{11}\frac{\partial w_1}{\partial x}\frac{\partial w}{\partial x}\frac{\partial^2w}{\partial x^2}+c_1E_{12}\left(2\left(\frac{\partial^2w}{\partial x\partial y}\right)^2+\frac{\partial^3w}{\partial x^2\partial y}\frac{\partial w}{\partial y}+\frac{\partial^3w}{\partial x\partial y^2}\frac{\partial w}{\partial x}\right)\\&+c_1E_{22}\left(\left(\frac{\partial^2w}{\partial y^2}\right)^2+\frac{\partial^3w}{\partial y^3}\frac{\partial w}{\partial y}\right)+A_{12}\frac{\partial w_1}{\partial y}\frac{\partial w}{\partial y}\frac{\partial^2w}{\partial x^2}\\&+2c_1E_{66}\left(\left(\frac{\partial^2w}{\partial x\partial y}\right)^2+\frac{\partial^3w}{\partial x\partial y^2}\frac{\partial w}{\partial x}+\frac{\partial^3w}{\partial x^2\partial y}\frac{\partial w}{\partial y}+\frac{\partial^2w}{\partial x^2}\frac{\partial^2w}{\partial y^2}\right)\\&+\left(A_{12}\frac{\partial w_1}{\partial x}\frac{\partial w}{\partial x}+A_{12}\frac{\partial w_1}{\partial y}\frac{\partial w}{\partial y}\right)\frac{\partial^2w}{\partial y^2}+2A_{66}\left(\frac{\partial w_1}{\partial x}\frac{\partial w}{\partial x}\right)\frac{\partial^2w}{\partial x\partial y}\\&+2A_{66}\frac{\partial w_1}{\partial x}\frac{\partial w}{\partial y}\frac{\partial^2w}{\partial x\partial y}+\frac{A_{11}}{2}\left(\frac{\partial w}{\partial x}\right)^2\frac{\partial^2w}{\partial x^2}+\frac{A_{12}}{2}\left(\frac{\partial w}{\partial y}\right)^2\frac{\partial^2w}{\partial x^2}\\&+\left[\frac{A_{12}}{2}\left(\frac{\partial w}{\partial x}\right)^2+\frac{A_{22}}{2}\left(\frac{\partial w}{\partial y}\right)^2\right]\frac{\partial^2w}{\partial y^2}+2c_2D_{55}+c_2^2F_{55}\frac{\partial\varphi_x}{\partial x}\frac{\partial\varphi_x}{\partial x}\\&+\left(+\frac{B_{11}}{R_x}+\frac{B_{12}}{R_y}-\frac{c_1E_{11}}{R_x}-\frac{c_1E_{12}}{R_y}+A_{55}\right)\frac{\partial\varphi_x}{\partial x}+2c_2D_{44}\frac{\partial\varphi_y}{\partial y}\\&+(c_1F_{11}-c_1^2H_{11})\frac{\partial^3\varphi_x}{\partial x^3}+2A_{66}\frac{\partial w}{\partial x}\frac{\partial w}{\partial y}\frac{\partial^2w}{\partial x\partial y}\\&+(c_1F_{12}+2c_1F_{66}-2c_1^2H_{66}-c_1^2H_{12})\frac{\partial^3\varphi_x}{\partial x\partial y^2}+\Xi=0\end{aligned} \tag{14}$$

$$
\begin{aligned}
&\left(B_{11}-c_1E_{11}\right)\frac{\partial^2 u}{\partial x^2}+\left(B_{66}-c_1E_{66}\right)\frac{\partial^2 u}{\partial y^2}+\left(B_{12}-c_1E_{12}\right)\frac{\partial^2 v}{\partial x\partial y}\\
&+\left(B_{66}-c_1E_{66}\right)\frac{\partial^2 v}{\partial x\partial y}+\left(B_{66}-c_1E_{66}\right)\left(\frac{\partial^2 w_1}{\partial y^2}\frac{\partial w}{\partial x}+\frac{\partial^2 w}{\partial y^2}\frac{\partial w_1}{\partial x}\right)\\
&+\left(B_{66}-c_1E_{66}\right)\left(\frac{\partial^2 w_1}{\partial x\partial y}\frac{\partial w}{\partial y}+\frac{\partial^2 w}{\partial x\partial y}\frac{\partial w_1}{\partial y}\right)+c_1\frac{E_{11}}{R_x}\frac{\partial w}{\partial x}\\
&+\left(B_{11}-c_1E_{11}\right)\left(\frac{\partial^2 w_1}{\partial x^2}\frac{\partial w}{\partial x}+\frac{\partial^2 w}{\partial x^2}\frac{\partial w_1}{\partial x}\right)+B_{11}\frac{\partial^2 w}{\partial x^2}\frac{\partial w}{\partial x}\\
&+\left(B_{12}-c_1E_{12}\right)\left(\frac{\partial^2 w_1}{\partial x\partial y}\frac{\partial w}{\partial y}+\frac{\partial^2 w}{\partial x\partial y}\frac{\partial w_1}{\partial y}\right)-c_1E_{11}\frac{\partial^2 w}{\partial x^2}\frac{\partial w}{\partial x}\\
&-\left(A_{55}-c_2^2F_{55}-c_1\frac{E_{12}}{R_y}+\frac{B_{11}}{R_x}+\frac{B_{12}}{R_y}\right)\frac{\partial w}{\partial x}-2c_1F_{11}\frac{\partial^2\varphi_x}{\partial x^2}\\
&+\left(B_{66}-c_1E_{66}\right)\left(\frac{\partial^2 w}{\partial y^2}\frac{\partial w}{\partial x}+\frac{\partial^2 w}{\partial x\partial y}\frac{\partial w}{\partial y}\right)+B_{12}\frac{\partial^2 w}{\partial x\partial y}\frac{\partial w}{\partial y}\\
&-c_1E_{12}\frac{\partial^2 w}{\partial x\partial y}\frac{\partial w}{\partial y}+\left(D_{66}-2c_1F_{66}+c_1^2H_{66}\right)\frac{\partial^2\varphi_x}{\partial y^2}\\
&-\left(A_{55}-c_2^2F_{55}\right)\varphi_x+\left(D_{11}+c_1^2H_{11}\right)\frac{\partial^2\varphi_x}{\partial x^2}-2c_1F_{12}\frac{\partial^2\varphi_y}{\partial x\partial y}\\
&+\left(D_{12}-2c_1F_{66}+c_1^2H_{66}\right)\frac{\partial^2\varphi_y}{\partial x\partial y}+\left(c_1^2H_{12}+D_{66}\right)\frac{\partial^2\varphi_y}{\partial x\partial y}\\
&=\overline{I}_2\frac{\partial^2 u}{\partial t^2}+\overline{I}_4\frac{\partial^2\varphi_x}{\partial t^2}-\overline{I}_5\frac{\partial^3 w}{\partial x\partial t^2},
\end{aligned}
\tag{15}
$$

$$
\begin{aligned}
&\left(B_{12}-c_1E_{12}+B_{66}-c_1E_{66}\right)\frac{\partial^2 u}{\partial x\partial y}-c_1E_{66}\frac{\partial^2 w_1}{\partial x^2}\frac{\partial w}{\partial y}+B_{66}\frac{\partial^2 v}{\partial x^2}\\
&+\left(B_{22}-c_1E_{22}\right)\frac{\partial^2 v}{\partial y^2}+B_{66}\frac{\partial^2 w_1}{\partial x^2}\frac{\partial w}{\partial y}\\
&+\left(B_{66}-c_1E_{66}\right)\left(\frac{\partial^2 w_1}{\partial x^2}\frac{\partial w}{\partial y}+\frac{\partial^2 w}{\partial x^2}\frac{\partial w_1}{\partial y}+\frac{\partial^2 w_1}{\partial x\partial y}\frac{\partial w}{\partial x}\right)\\
&\left(B_{66}-c_1E_{66}\right)\left(\frac{\partial^2 w}{\partial x\partial y}\frac{\partial w_1}{\partial x}\right)+\left(B_{11}-c_1E_{11}\right)\frac{\partial^2 w}{\partial y^2}\frac{\partial w}{\partial y}\\
&+\left(B_{22}-c_1E_{22}\right)\left(\frac{\partial^2 w_1}{\partial y^2}\frac{\partial w}{\partial y}+\frac{\partial^2 w}{\partial y^2}\frac{\partial w_1}{\partial y}\right)\\
&+\left(B_{12}-c_1E_{12}\right)\left(\frac{\partial^2 w_1}{\partial x\partial y}\frac{\partial w}{\partial x}+\frac{\partial^2 w}{\partial x\partial y}\frac{\partial w_1}{\partial x}\right)\\
&-\left(A_{44}-c_2^2F_{44}-c_1\frac{E_{12}}{R_x}-c_1\frac{E_{22}}{R_y}+\frac{B_{12}}{R_x}+\frac{B_{22}}{R_y}\right)\frac{\partial w}{\partial y}\\
&+\left(B_{66}-c_1E_{66}\right)\left(\frac{\partial^2 w}{\partial x^2}\frac{\partial w}{\partial y}+\frac{\partial^2 w}{\partial x\partial y}\frac{\partial w}{\partial x}\right)+\left(B_{12}-c_1E_{12}\right)\frac{\partial^2 w}{\partial x\partial y}\frac{\partial w}{\partial x}\\
&+\left(c_1^2H_{12}+D_{66}\right)\frac{\partial^2\varphi_x}{\partial x\partial y}+\left(D_{12}-2c_1F_{12}-2c_1F_{66}+c_1^2H_{66}\right)\frac{\partial^2\varphi_x}{\partial x\partial y}\\
&+\left(D_{22}-2c_1F_{22}+c_1^2H_{22}\right)\frac{\partial^2\varphi_y}{\partial y^2}+c_1^2H_{66}\frac{\partial^2\varphi_y}{\partial x^2}\\
&+\left(D_{66}-2c_1F_{66}\right)\frac{\partial^2\varphi_y}{\partial x^2}-\left(A_{55}-c_2^2F_{44}\right)\varphi_y\\
&=\overline{I}_2^*\frac{\partial^2 v}{\partial t^2}+\overline{I}_4^*\frac{\partial^2\varphi_y}{\partial t^2}-\overline{I}_5^*\frac{\partial^3 w}{\partial y\partial t^2}.
\end{aligned}
\tag{16}
$$

in which (She and Ding 2023)

$$
\begin{aligned}
&\left\{A_{ij},B_{ij},D_{ij},E_{ij},F_{ij},H_{ij}\right\}=\int_{-h/2}^{h/2}Q_{ij}(z,T)\left\{1,z,z^2,z^3,z^4,z^6\right\}\mathrm{d}z,\\
&(i,j=1,2,6),\\
&\left\{A_{ij},D_{ij},F_{ij},\right\}=\int_{-h/2}^{h/2}Q_{ij}(z,T)\left\{1,z^2,z^4\right\}\mathrm{d}z,\quad(i,j=4,5).\\
&\left\{I_1,I_2,I_3,I_4,I_5,I_7\right\}=\int_{-h/2}^{h/2}\rho(z)\left\{1,z,z^2,z^3,z^4,z^6\right\}\mathrm{d}z\\
&\overline{I}_1=I_1+\frac{2I_2}{R_x},\ \overline{I}_1^*=I_1+\frac{2I_2}{R_y},\overline{I}_2=I_2+\frac{I_3}{R_x}-c_1I_4-c_1\frac{I_5}{R_x},\\
&\overline{I}_2^*=I_2+\frac{I_3}{R_y}-c_1I_4-c_1\frac{I_5}{R_y},\overline{I}_3=c_1I_4+c_1\frac{I_5}{R_x},\\
&\overline{I}_3^*=c_1I_4+c_1\frac{I_5}{R_y},\overline{I}_4=I_3-2c_1I_5+c_1^2I_7,\ \ \overline{I}_4^*=I_3-2c_1I_5+c_1^2I_7,\\
&\overline{I}_5=c_1I_5-c_1^2I_7,\ \ \overline{I}_5^*=c_1I_5-c_1^2I_7,
\end{aligned}
\tag{17}
$$

$$
\begin{aligned}
\Xi=&\left(c_2^2F_{44}+\frac{B_{12}}{R_x}+\frac{B_{22}}{R_y}-\frac{c_1E_{12}}{R_x}-\frac{c_1E_{22}}{R_y}+A_{44}\right)\frac{\partial\varphi_y}{\partial y}\\
&+\left(c_1F_{22}-c_1^2H_{22}\right)\frac{\partial^3\varphi_y}{\partial y^3}+\left(c_1F_{12}+2c_1F_{66}\right)\frac{\partial^3\varphi_y}{\partial x^2\partial y}\\
&-\left(2c_1^2H_{66}+c_1^2H_{12}\right)\frac{\partial^3\varphi_y}{\partial x^2\partial y}+A_{11}\frac{\partial u}{\partial x}\frac{\partial^2 w}{\partial x^2}+A_{12}\frac{\partial u}{\partial x}\frac{\partial^2 w}{\partial y^2}\\
&+2A_{66}\frac{\partial u}{\partial y}\frac{\partial^2 w}{\partial x\partial y}+A_{12}\frac{\partial v}{\partial y}\frac{\partial^2 w}{\partial x^2}+A_{12}\frac{\partial v}{\partial y}\frac{\partial^2 w}{\partial y^2}\\
&+2A_{66}\frac{\partial v}{\partial x}\frac{\partial^2 w}{\partial x\partial y}+\left(B_{11}-c_1E_{11}\right)\frac{\partial\varphi_x}{\partial x}\frac{\partial^2 w}{\partial x^2}\\
&+\left(B_{12}-c_1E_{12}\right)\frac{\partial\varphi_x}{\partial x}\frac{\partial^2 w}{\partial y^2}+\left(2B_{66}-2c_1E_{66}\right)\frac{\partial\varphi_x}{\partial y}\frac{\partial^2 w}{\partial x\partial y}\\
&+\left(B_{12}-c_1E_{12}\right)\frac{\partial\varphi_y}{\partial y}\frac{\partial^2 w}{\partial x^2}+\left(B_{22}-c_1E_{22}\right)\frac{\partial\varphi_y}{\partial y}\frac{\partial^2 w}{\partial y^2}\\
&+\left(2B_{66}-2c_1E_{66}\right)\frac{\partial\varphi_y}{\partial x}\frac{\partial^2 w}{\partial x\partial y}+q=I_1\frac{\partial^2 w}{\partial t^2}+\overline{I}_3\frac{\partial^3 u}{\partial x\partial t^2}\\
&+\overline{I}_3^*\frac{\partial^3 v}{\partial y\partial t^2}+c_1\overline{I}_5\frac{\partial^3\varphi_x}{\partial x\partial t^2}+c_1\overline{I}_5^*\frac{\partial^3\varphi_y}{\partial y\partial t^2}-c_1^2I_7\left(\frac{\partial^4 w}{\partial x^2\partial t^2}\right)\\
&-c_1^2I_7\frac{\partial^4 w}{\partial y^2\partial t^2}.
\end{aligned}
\tag{18}
$$

4. Solution method

In this article, we consider simply supported boundary conditions and assume that the external excitation load is a harmonic load, i.e., $q=q\cos(\Omega t)$. Due to the fact that this article only considers simply supported boundary conditions, this is one of the limitations of this article. In addition, we assume that the displacements take the following form (She and Ding 2023),

$$
\begin{aligned}
u&=\sum_{m=1}^{\infty}\sum_{n=1}^{\infty}\mathbf{U(t)}\cos\left(\frac{\pi mx}{a}\right)\sin\left(\frac{\pi ny}{b}\right),\\
v&=\sum_{m=1}^{\infty}\sum_{n=1}^{\infty}\mathbf{V(t)}\sin\left(\frac{\pi mx}{a}\right)\cos\left(\frac{\pi ny}{b}\right),\\
w&=\sum_{m=1}^{\infty}\sum_{n=1}^{\infty}\mathbf{W(t)}\sin\left(\frac{\pi mx}{a}\right)\sin\left(\frac{\pi ny}{b}\right),\\
w_1&=\sum_{m=1}^{\infty}\sum_{n=1}^{\infty}\mathbf{W_1}\sin\left(\frac{\pi mx}{a}\right)\sin\left(\frac{\pi ny}{b}\right),\\
\varphi_x&=\sum_{m=1}^{\infty}\sum_{n=1}^{\infty}\mathbf{\Phi_x(t)}\cos\left(\frac{\pi mx}{a}\right)\sin\left(\frac{\pi ny}{b}\right),\\
\varphi_y&=\sum_{m=1}^{\infty}\sum_{n=1}^{\infty}\mathbf{\Phi_y(t)}\sin\left(\frac{\pi mx}{a}\right)\cos\left(\frac{\pi ny}{b}\right).
\end{aligned}
\tag{19}
$$

Because the transverse vibration plays a decisive role in the vibration problem, the influence of the inertia terms of axial and rotation vibrations can be ignored. Therefore, we only consider the transverse vibration. Upon substitution of Eq. (19) into Eqs. (12) - (16), a set of six ordinary differential equations can be extracted, these equations are given in Appendix. By eliminating the $\mathbf{U(t)}$, $\mathbf{V(t)}$, $\mathbf{\Phi_x(t)}$, and $\mathbf{\Phi_y(t)}$, we can get the classical Duffing equation, which is the same as the previous work (She and Ding 2023), and then, the solution can be determined with the aid of modified Lindstedt Poincare method, by referring to Ref. (Chen and Cheung 1996), we can obtain the asymptotic solution for the resonance problem.

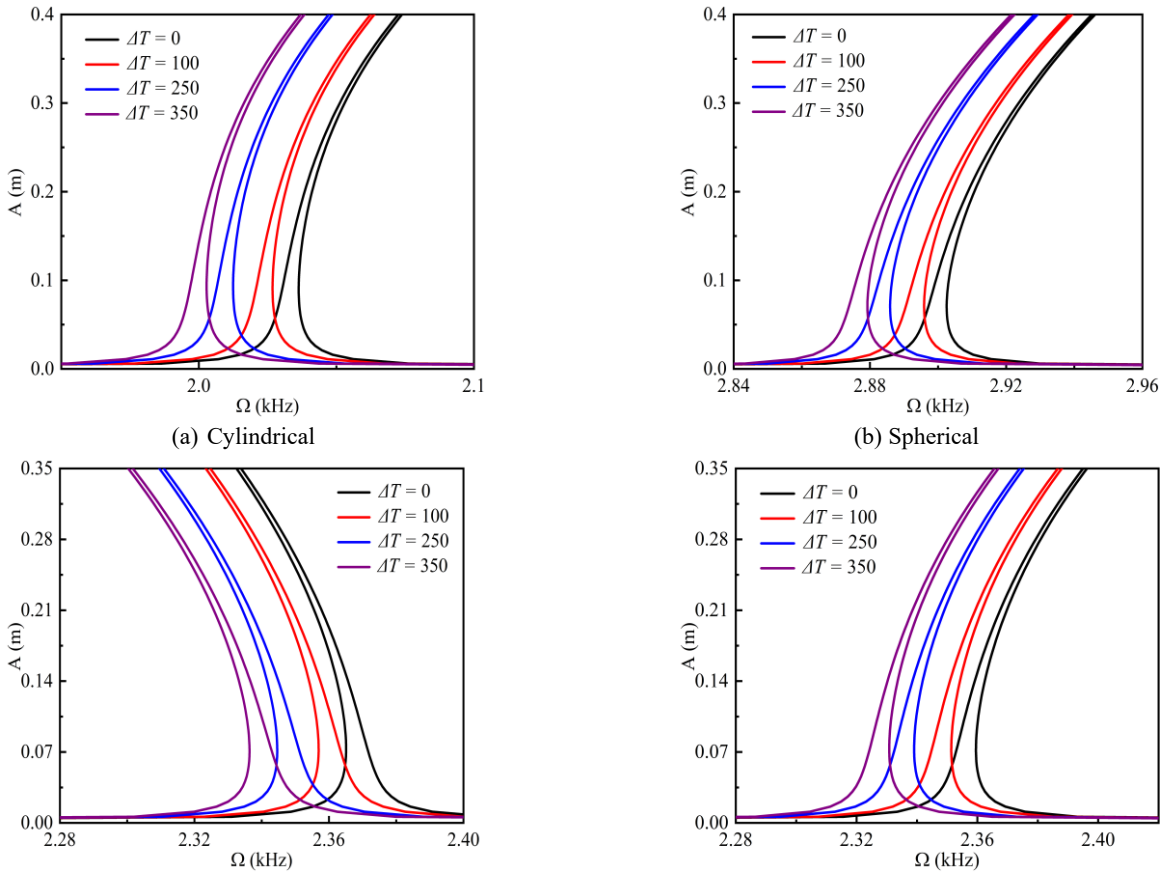

(a) Cylindrical (b) Spherical

(c) Hyperbolic (d) Elliptical

Fig. 3 Resonance diagrams for different temperature changes at h = 0.45 m, a =b=R = 4.5 m, P=1 MPa, W_{gpl}=0.01,W_1=0.5, porosity-I,GPL-A, q =3MPa, e_1=0.2, (m,n)=(1,1)

Table 1 Comparative analysis for the dimensionless linear natural frequencies $\Omega=\omega R(\rho_1/E_1)^{1/2}$ of a metal foam cylindrical shell

e_1	n = 3		n = 4	
	Ref. (Wang *et al.* 2019)	Present	Ref. (Wang *et al.* 2019)	Present
0	1.2366	1.2434	1.2300	1.2410
0.2	1.2102	1.2159	1.2048	1.2139
0.4	1.1836	1.1879	1.1795	1.1862
0.6	1.1585	1.1609	1.1560	1.1596

5. Numerical analyses

To validate the present paper, a metal foam cylindrical shell is taken into account, and Table 1 gives the dimensionless linear natural frequencies $\Omega = \omega R(\rho_1/E_1)^{1/2}$ for comparison. From Table 1, our results are basically consistent with those given in the existing literature (Wang *et al.* 2019), thus verifying the correctness of this study.

In following part, the adopted material is given in Table 2.

Fig. 3 depicts the effect of temperature changes ΔT(K) on the resonance diagrams of hyperbolic- ($R_x = R$, $R_y = -R$), elliptical- ($R_x = R$, $R_y = 2R$), spherical- ($R_x = R$, $R_y = R$), and cylindrical- ($R_x = R$, $R_y = \rightarrow\infty$) shells. In the figure, the x-axis represents the exciting frequency, and the y-axis represents the deflection. It can be seen that, as the temperature goes up, the resonance position can be advanced. Thus, if we ignore the effect of temperature load, we will overestimate the resonance position. Therefore, it is necessary to consider the effect of temperature load in practical engineering. Besides, we can see that the ellipsoidal and hyperbolic shells have almost the similar resonance positions. Moreover, the forced vibration curve for the hyperbolic-shell is bent to lower frequency (soft spring).

Fig. 4 shows the effects of material properties on the resonance diagrams of hyperbolic- (Rx = R, Ry = −R), elliptical- (Rx = R, Ry = 2R), spherical- (Rx = R, Ry = R), and cylindrical- (Rx = R, Ry = →∞) shells. As seen, (a) GPL-C shells first resonates. (b) Porosity-II shells first resonates. (c) With the increase of GPL weight fraction, the resonance position will be delayed. (d) On the contrary, the natural frequency of the shell decreases with the increase of the porosity coefficient, so the resonance position will be advanced.

In Fig. 5, we investigate the effect of geometric imperfection. As shown in the figure, when W_1=0, the greater the amplitude is, the greater the nonlinear natural frequency becomes. The amplitude frequency response relationship shows the property of hard spring. With the

Table 2 Material properties (Wang and Zhang 2022)

Materials	Properies	P_{-1}	P_0	P_1	P_2	P_3
Nichel	E_m (Pa)	0	223.95×10^{9}	-2.974×10^{-4}	-3.998×10^{-9}	0
	v_m	0	0.28	0	0	0
	ρ_m (kg/m^3)	0	8908	0	0	0
	α_m (1/K)	0	9.9209×10^{-6}	8.7056×10^{-4}	0	0
GPLs	E_{gpl}	0	1087.8×10^{9}	-0.261×10^{9}	0	0
	v_{gpl}	0	0.186	0	0	0
	ρ_{gpl} (kg/m^3)	0	1060	0	0	0
	α_{gpl} (1/K)	0	13.92×10^{-6}	-0.0299×10^{-6}	0	0

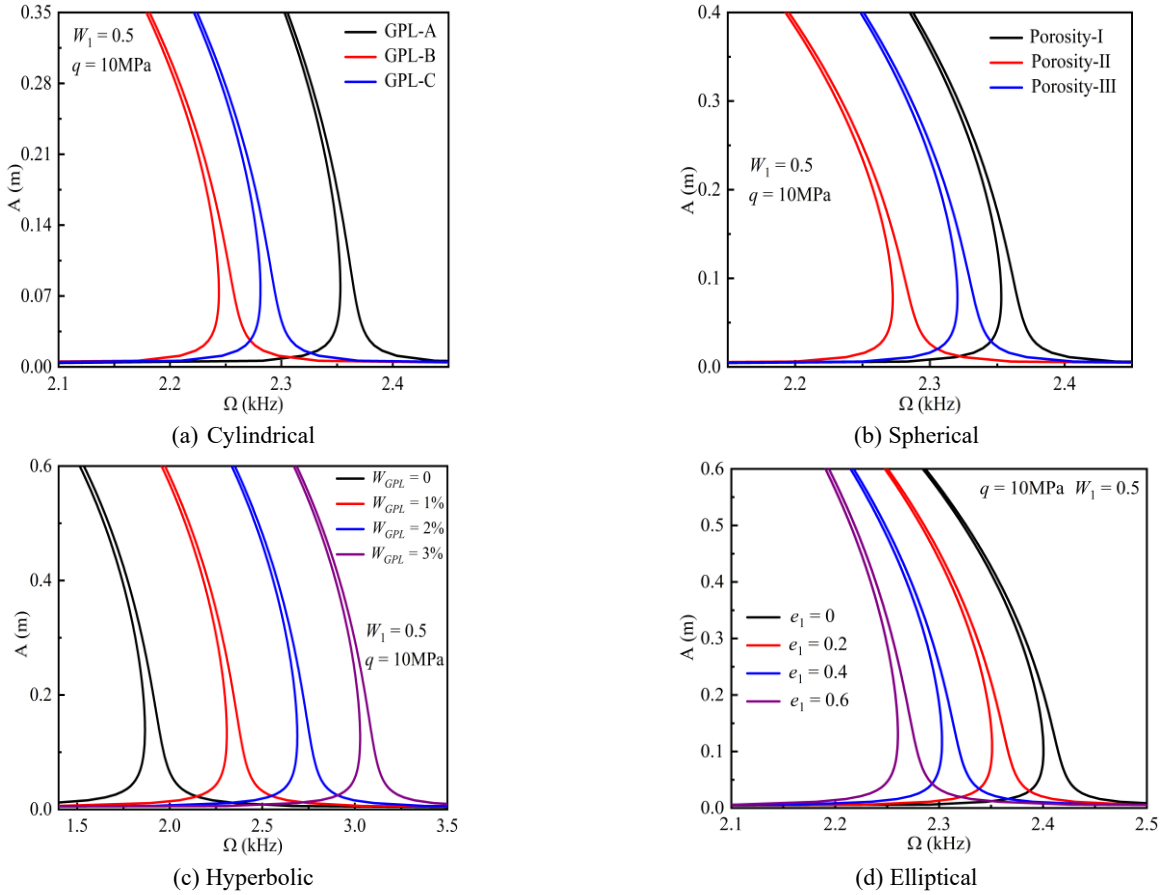

(a) Cylindrical (b) Spherical

(c) Hyperbolic (d) Elliptical

Fig. 4 Resonance diagrams for material properties of hyperbolic shells at W_{gpl} = 0.01, h = 0.45 m, a =b=R= 4.5 m, P=1 MPa, e_1 = 0.2,ΔT = 100 K, (m,n)=(1,1); the effect of (a) GPLs distribution patterns, (b) porosity distribution patterns, (c) GPLs weight fraction and (d) the porosity coefficient

increase of initial geometric defect, especially when W_1=0.8, the larger the amplitude is, the smaller the nonlinear natural frequency is. At this time, the amplitude frequency response relationship shows the property of soft spring. In addition, we can also find that the resonance position hardly changes with the increase of initial geometric imperfection.

Fig. 6 describes the influence of prestress on the amplitude frequency response curve of GPLRMFs doubly curved shells. When prestress is applied to GPLRMFs hyperbolic shells, the natural frequency of the structure increases with the increase of prestress, thus delaying the resonance position of GPLRMFs hyperbolic shells.

6. Conclusions

Through the dynamic analysis of the frequency-amplitude response curves, the following conclusions can be drawn.

(1) The resonance position will be advanced with the increase of temperature. If we ignore the effect of temperature load, we will overestimate the resonance position.

(2) The spherical shell has the maximum resonant position, and the forced vibration curve for the hyperbolic-shell is bent to lower frequency.

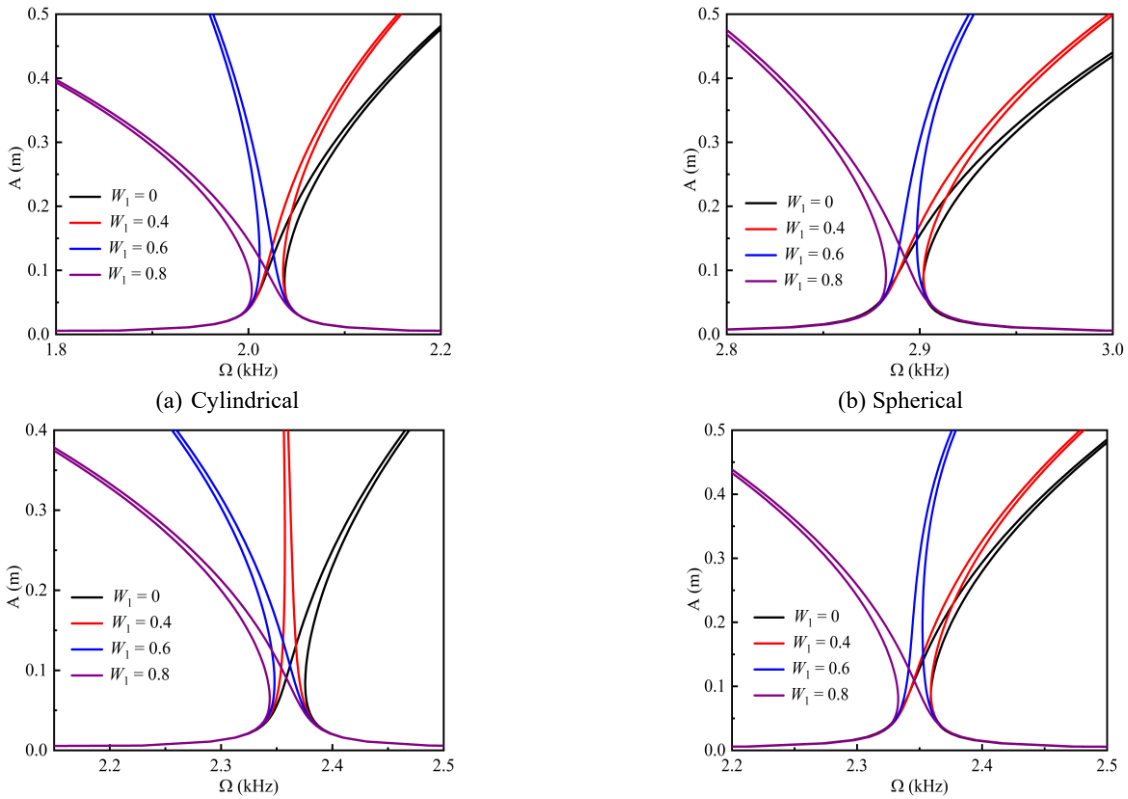

(a) Cylindrical (b) Spherical

(c) Hyperbolic (d) Elliptical

Fig. 5 Resonance diagrams at W_{gpl} = 0.01, h = 0.45m, a =b=R = 4.5 m, P=1MPa, e_1 = 0.2, porosity-I,GPL-A, q =10 MPa,ΔT = 100 K, (m,n)=(1,1)

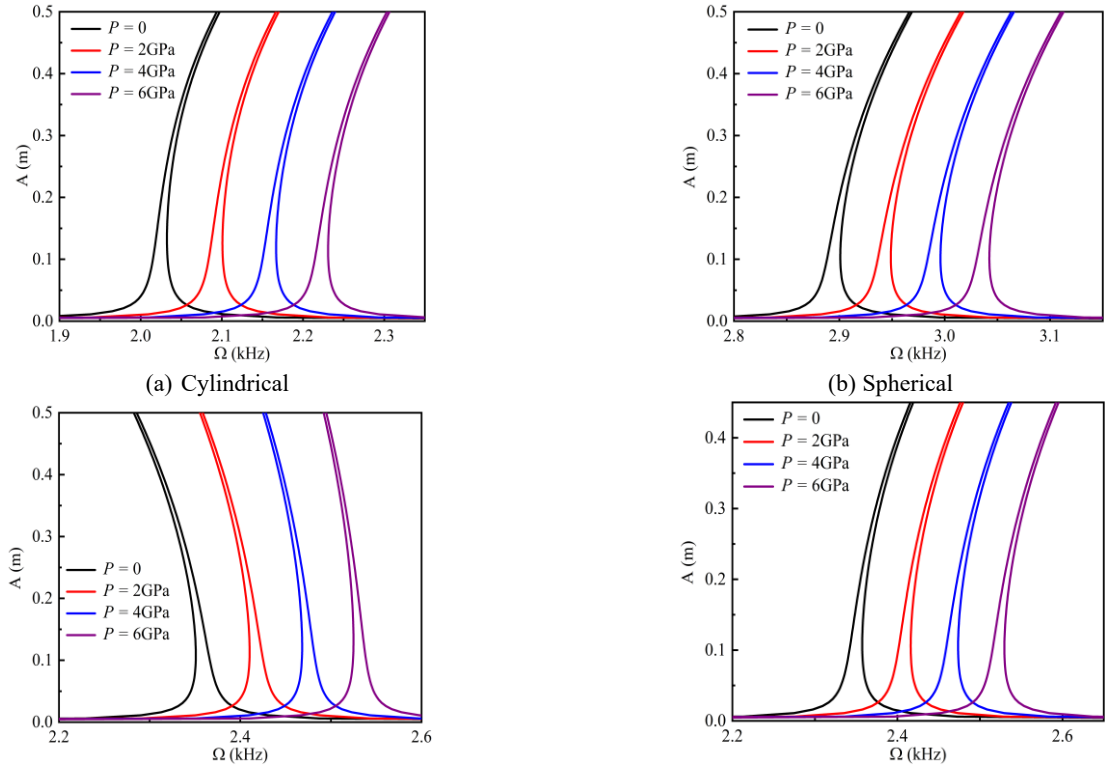

(a) Cylindrical (b) Spherical

(c) Hyperbolic (d) Elliptical

Fig. 6 Resonance diagrams at h = 0.45 m, a =b=R= 4.5 m, e_1=0.2, W_{gpl}=0.01,W_l=0.5, porosity-I,GPL-A, q =10 MPa, ΔT = 100 K, (m,n)=(1,1)

(3) For GPLs distribution patterns, GPL-C shells first resonates, followed by GPL-B and GPL-A shells. For porosity distribution patterns, Porosity-II shells first resonates, followed by Porosity-III and Porosity-I shells. For GPLs weight fraction, with the increase of GPL weight fraction, the resonance position will be delayed. For the porosity coefficient, with the increase of the porosity coefficient, the resonance position will be advanced.

References

Abdelrahman, A.A., Shanab, R.A., Esen, I. and Eltaher, M.A. (2022), "Effect of moving load on dynamics of nanoscale Timoshenko CNTs embedded in elastic media based on doublet mechanics theory", *Steel. Compos. Struct*., **44**(2), 241-256. https://doi.org/10.12989/scs.2022.44.2.241.

Alazwari, M.A., Daikh, A.A., Houari, M.S., Tounsi, A. and Eltaher, M.A. (2021), "On static buckling of multilayered carbon nanotubes reinforced composite nanobeams supported on non-linear elastic foundations", *Steel. Compos. Struct*., **40**(3), 389-404. https://doi.org/10.12989/scs.2021.40.3.389.

Ahmadi, H. and Foroutan, K. (2019), "Nonlinear vibration of stiffened multilayer FG cylindrical shells with spiral stiffeners rested on damping and elastic foundation in thermal environment", *Thin. Wall. Struct*., **145**, 106388. https://doi.org/10.1016/j.tws.2019.106388.

Ahmed, R.A., Khalaf, B.S., Raheef, K.M., Fenjan, R.M. and Faleh, N.M. (2021), "Investigating dynamic response of nonlocal functionally graded porous piezoelectric plates in thermal environment", *Steel. Compos. Struct*., **40**(2), 243-254 .https://doi.org/10.12989/scs.2021.40.2.243.

Aris, H. and Ahmadi, H. (2022), "Combination resonance analysis of imperfect functionally graded conical shell resting on nonlinear viscoelastic foundation in thermal environment under multi-excitation", *J. Vib. Control*., **28**, 15-16. https://doi.org/10.1177/10775463211006527.

Ahmadi, H. and Foroutan, K. (2021), "Nonlinear buckling analysis of FGP shallow spherical shells under thermomechanical condition", *Steel. Compos. Struct*., **40**(4), 555-570. https://doi.org/10.12989/scs.2021.40.4.555.

Ahmadi, H. and Foroutan, K. (2020), "Nonlinear static and dynamic thermal buckling analysis of imperfect multilayer FG cylindrical shells with an FG porous core resting on nonlinear elastic foundation", *J. Therm. Stresses*., **43**(5), 629-649. https://doi.org/10.1080/01495739.2020.1727802.

Abuteir. B.W., Harkati, E., Boutagouga, D., Mamouri, S. and Djeghaba, K. (2021), "Thermo-mechanical nonlinear transient dynamic and dynamic-Buckling analysis of functionally graded material shell structures using an implicit conservative/decaying time integration scheme", *Mech. Adv. Mater. Struc*., https://doi.org/ 10.1080/15376494.2021.1964115.

Abuteir, B.W. and Boutagouga, D. (2022), "Free-vibration response of functionally graded porous shell structures in thermal environments with temperature-dependent material properties", *Acta. Mech*., **233**(11), 4877-4901. https://doi.org/10.1007/s00707-022-03351-y.

Babaei, H. (2022a), "Nonlinear analysis of size-dependent frequencies in porous FG curved nanotubes based on nonlocal strain gradient theory", *Eng. Struct*., **38**(3), 1717-1734. https://doi.org/10.1007/s00366-021-01317-7.

Babaei, H. (2022b), "Free vibration and snap-through instability of FG-CNTRC shallow arches supported on nonlinear elastic foundation", *Appl. Math. Comput*., **413**, 126606. https://doi.org/10.1016/j.amc.2021.126606.

Babaei, H. and Eslami, M.R. (2021a), "Nonlinear analysis of thermal-mechanical coupling bending of FGP infinite length cylindrical panels based on PNS and NSGT", *Appl. Math. Model*., **91**, 1061-1080. https://doi.org/10.1016/j.apm.2020.10.004.

Babaei, H. and Eslami, M.R. (2021b), "Nonlinear analysis of thermal-mechanical coupling bending of clamped FG porous curved micro-tubes", *J. Therm. Stresses*, **44**(4), 409-432. https://doi.org/10.1080/01495739.2020.1870417.

Baghlani, A., Khayat, M. and Dehghan, S.M. (2020), "Free vibration analysis of FGM cylindrical shells surrounded by Pasternak elastic foundation in thermal environment considering fluid-structure interaction", *Appl. Math. Model*., **78**, 550-575. https://doi.org/10.1016/j.apm.2019.10.023.

Basha, M., Daikh, A.A., Melaibari, A., Wagih, A., Othman, R., Almitani, K.H., Hamed, M.A., Abdelrahman, A. and Eltaher, M.A. (2022), "Nonlocal strain gradient theory for buckling and bending of FG-GRNC laminated sandwich plates", *Steel. Compos. Struct*., **43**(5), 639-660. https://doi.org/10.12989/scs.2022.43.5.639.

Chan, D.Q., Quan, T.Q., Kim, S.E. and Duc, N.D. (2019), "Nonlinear dynamic response and vibration of shear deformable piezoelectric functionally graded truncated conical panel in thermal environments", *Eur. J. Mech. A-Solid*., **77**, 103795. https://doi.org/10.1016/j.euromechsol.2019.103795.

Chen, X., Zhao, J.L., She, G.L., Jing, Y., Luo, J. and Pu, H.Y. (2022a), "On wave propagation of functionally graded CNT strengthened fluid-conveying pipe in thermal environment", *Eur. Phys. J. Plus*., **137**(10), 1158. https://doi.org/10.1140/epjp/s13360-022-03234-0.

Chen, X., Zhao, J.L., She, G.L., Jing, Y., Pu, H.Y. and Luo, J. (2022b), "Nonlinear free vibration analysis of functionally graded carbon nanotube reinforced fluid-conveying pipe in thermal environment", *Steel. Compos. Struct*., **45**(5), 641-652. https://doi.org/10.12989/scs.2022.45.5.641.

Chai, Q.D. and Wang, Y.Q. (2022), "Traveling wave vibration of graphene platelet reinforced porous joined conical-cylindrical shells in a spinning motion", *Eng. Struct*., **252**, 113718. https://doi.org/10.1016/j.engstruct.2021.113718.

Chen, S.H. and Cheung, Y.K. (1996), "A Modified Lindstedt–Poincaré Method for a Strongly Nonlinear System with Quadratic and Cubic Nonlinearities", *Shock. Vib*., **3**(4), 279-285. https://doi.org/10.1155/1996/231241.

Daikh, A.A., Houari, M.S.A., Karami, B., Eltaher, M.A., Dimitri, R. and Tornabene, F. (2021), "Buckling analysis of CNTRC curved sandwich nanobeams in thermal environment", *Appl. Sci*., **11**(7), 3250. https://doi.org/10.3390/app11073250.

Dastjerdi, S., Akgoz, B., Civalek, O., Malikan, M. and Eremeyev, V. A. (2020), "On the non-linear dynamics of torus-shaped and cylindrical shell structures", *Int. J. Eng. Sci*., **156**, 103371. https://doi.org/ 10.1016/j.ijengsci.2020.103371.

Dat, N.D., Khoa, N.D., Nguyen, P.D. and Duc, N.D. (2020), "An analytical solution for nonlinear dynamic response and vibration of FG-CNT reinforced nanocomposite elliptical cylindrical shells resting on elastic foundations", *Zamm-Z. Angew. Math. Me*., **100**(1), UNSP e201800238. https://doi.org/10.1002/zamm.201800238.

Ding, H.X., Eltaher, M.A. and She, G.L. (2023a), "Nonlinear low-velocity impact of graphene platelets reinforced metal foams cylindrical shell: Effect of spinning motion and initial geometric imperfections", *Aerosp. Sci. Technol.*, **140**, 108435. https://doi.org/10.1016/j.ast.2023.108435.

Ding, H.X. and She, G.L. (2021), "A higher-order beam model for the snap-buckling analysis of FG pipes conveying fluid", *Struct. Eng. Mech*., **80**(1), 63-72. https://doi.org/10.12989/sem.2021.80.1.063.

Ding, H.X., She, G.L. and Zhang, Y.W. (2022a), "Nonlinear buckling and resonances of functionally graded fluid-conveying

pipes with initial geometric imperfection", *Eur. Phys. J. Plus*, **137**, 1329. https://doi.org/10.1140/epjp/s13360-022-03570-1.

Ding, H.X. and She, G.L. (2023a), "Nonlinear resonance of axially moving graphene platelet-reinforced metal foam cylindrical shells with geometric imperfection", *Arch. Civil Mech. Eng*., **23**, 97. https://doi.org/10.1007/s43452-023-00634-6.

Ding, H.X. and She, G.L. (2023b), "Nonlinear primary resonance behavior of graphene platelets reinforced metal foams conical shells under axial motion", *Nonlinear Dynam.*, https://doi.org/10.1007/s11071-023-08564-x.

Ding, H.X., Zhang, Y.W. and She, G.L. (2022b), "On the resonance problems in FG-GPLRC beams with different boundary conditions resting on elastic foundations", *Comput. Concrete*, **30**(6), 433-443. https://doi.org/10.12989/cac.2022.30.6.433.

Ding, H.X., Zhang, Y.W. and She, G.L. (2023b), "Propagation characteristics of guided waves in CNTRCbs plates resting on elastic foundations in a thermal environment", *Waves in Random and Complex Media*, https://doi.org/10.1080/17455030.2023.2235611.

Ding, H.X., Liu, H.B., She, G.L. and Wu, F. (2023c), "Wave propagation of FG-CNTRC plates in thermal environment using the high-order shear deformation plate theory", *Comput. Concrete*, **32**(2), 207-215. https://doi.org/10.12989/cac.2023.32.2.207.

Duc, N.D., Khoa, N.D. and Thiem, H. T. (2018), "Nonlinear thermo-mechanical response of eccentrically stiffened Sigmoid FGM circular cylindrical shells subjected to compressive and uniform radial loads using the Reddy's third-order shear deformation shell theory", *Mech. Adv. Mater. Struc*., **25**(13), 1156-1167. https://doi.org/ 10.1080/15376494.2017.1341581.

Duc, N.D., Tuan, N.D., Tran, P., Quan, T.Q. and Thanh, N.V. (2019), "Nonlinear dynamic response and vibration of imperfect eccentrically stiffened sandwich third-order shear deformable FGM cylindrical panels in thermal environments", *J. Sandw. Struct. Mater*., **21**(8), 2816-2845. https://doi.org/10.1177/1099636217725251.

Ebrahimi, F., Hashemabadi, D., Habibi, M. and Safarpour, H. (2020), "Thermal buckling and forced vibration characteristics of a porous GNP reinforced nanocomposite cylindrical shell", *Microsyst. Technol*., **26**(2), 461-473. https://doi.org/10.1007/s00542-019-04542-9.

Emadi, M., Nejad, M.Z., Ziaee, S. and Hadi, A. (2021), "Buckling analysis of arbitrary two-directional functionally graded nano-plate based on nonlocal elasticity theory using generalized differential quadrature method", *Steel Compos. Struct*., **39**(5) 565-581. https://doi.org/10.12989/scs.2021.39.5.565.

Emam, S.A., Eltaher, M.A., Khater, M.E. and Abdalla, W.S. (2018), "Postbuckling and free vibration of multilayer imperfect nanobeams under a pre-stress load", *Appl. Sci*., **8**(11), 2238. https://doi.org/10.3390/app8112238.

Esen, I., Daikh, A.A. and Eltaher, M.A. (2022), "Dynamic response of nonlocal strain gradient FG nanobeam reinforced by carbon nanotubes under moving point load", *Eur. Phys. J. Plus*, **136**(4), 1-22. https://doi.org/10.1140/epjp/s13360-021-01419-7.

Foroutan, K. and Ahmadi, H. (2022), "Nonlinear parametric vibration of imperfect SSMFG cylindrical shells in thermal environment including internal and subharmonic resonances", *Mech. Adv. Mater. Struc*., **29**(24), 3499-3522. https://doi.org/10.1080/15376494.2021.1904526.

Foroutan, K. and Dai, L. M. (2022), "Static and dynamic thermal post-buckling analysis of imperfect sigmoid FG cylindrical shells resting on a non-uniform elastic foundation", *Eur. J. Mech. A-Solid*., **97**, 104770. https://doi.org/10.1016/j.euromechsol.2022.104770.

Fu, T., Wu, X., Xiao, Z.M. and Chen, Z.B. (2020), "Thermoacoustic response of porous FGM cylindrical shell surround by elastic foundation subjected to nonlinear thermal loading", *Thin. Wall. Struct*., **156**, 106996. https://doi.org/10.1016/j.tws.2020.106996.

Gan, L.L. and She, G.L. (2023), "Nonlinear snap-buckling and resonance of FG-GPLRC curved beams with different boundary conditions", *Geomech. Eng*., **32**(5), 541-551. https://doi.org/10.12989/gae.2023.32.5.541.

Gan, L.L., Xu, J.Q. and She, G.L. (2023), "Wave propagation of graphene platelets reinforced metal foams circular plates", *Struct. Eng. Mech*., **85**(5), 645-654. https://doi.org/10.12989/sem.2023.85.5.645.

Hajilak, Z.E., Pourghader, J., Hashemabadi, D., Bagh, F.S., Habibi, M. and Safarpour, H. (2019), "Multilayer GPLRC composite cylindrical nanoshell using modified strain gradient theory", *Mech. Based. Des. Struc*., **47**(5), 521-545. https://doi.org/ 10.1080/15397734.2019.1566743.

Hendi, A., Eltaher, M.A, Mohamed, S.A. and Attia, M. (2022), "Nonlinear thermal vibration of pre/post-buckled two-dimensional FGM tapered microbeams based on a higher order shear deformation theory", *Steel Compos. Struct*., **41**(6), 787-802. https://doi.org/10.12989/scs.2021.41.6.787.

Heydarpour, Y., Mohammadzaheri, M., Ghodsi, M., Soltani, P., AlJahwari, F., Bahadur, I. and Al-Amri, B. (2020), "Application of the hybrid DQ- Heaviside-NURBS method for dynamic analysis of FG-GPLRC cylindrical shells subjected to impulse load", *Thin. Wall. Struct*., **155**, 106914. https://doi.org/10.1016/j.tws.2020.106914.

Hong, C.C. (2020), "Free vibration frequency of thick FGM spherical shells with simply homogeneous equation by using TSDT", *J. Braz. Soc. Mech. Sci*., **42**(4), 159. https://doi.org/10.1007/s40430-020-2248-z.

Hong, C.C. (2021), "Vibration frequency of thick functionally graded material cylindrical shells with fully homogeneous equation and third-order shear deformation theory under thermal environment", *J. Vib. Control*., **27**(17-18), 2004-2017. https://doi.org/ 10.1177/1077546320951663.

Karimiasl, M., Ebrahimi, F. and Akgoz, B. (2019), "Buckling and post-buckling responses of smart doubly curved composite shallow shells embedded in SMA fiber under hygro-thermal loading", *Compos. Struct*., **223**, 110988. https://doi.org/10.1016/j.compstruct.2019.110988.

Kitipornchai, S., Chen, D. and Yang, J. (2017), "Free vibration and elastic buckling of functionally graded porous beams reinforced by graphene platelets", *Mater. Design*, **116**, 656-665. https://doi.org/10.1016/j.matdes.2016.12.061.

Li, X., Chen, X.C. and Jiang, W. (2022), "Dynamic stability of graded graphene reinforced truncated conical shells under both periodic spinning speeds and axial loads considering thermal effects", *Eng. Struct*., **256**, 113963. https://doi.org/10.1016/j.engstruct.2022.113963.

Li, Y.P., She, G.L., Gan, L.L. and Liu, H.B. (2023), "Nonlinear thermal post-buckling analysis of graphene platelets reinforced metal foams plates with initial geometrical imperfection", *Steel. Compos, Struct*., **46**(5), 649-658. https://doi.org/10.12989/scs.2023.46.5.649.

Li, W., Hao, Y. X., Zhang, W. and Yang, H. (2021), "Resonance response of clamped functionally graded cylindrical shells with initial imperfection in thermal environments", *Compos. Struct*., **259**, 113245. https://doi.org/10.1016/j.compstruct.2020.113245.

Liu, B., Guo, M., Liu, C.Y. and Xing, Y. F. (2019), "Free vibration of functionally graded sandwich shallow shells in thermal environments by a differential quadrature hierarchical finite element method", *Compos. Struct*., **225**, 111173. https://doi.org/10.1016/j.compstruct.2019.111173.

Lu, L., She, G.L. and Guo, X. (2021), "Size-dependent postbuckling analysis of graphene reinforced composite microtubes with geometrical imperfection", *Int. J. Mech. Sci*.,

199, 106428. https://doi.org/10.1016/j.ijmecsci.2021.106428.

Maji, P., Rout, M. and Karmakar, A. (2020), "Free vibration response of carbon nanotube reinforced pretwisted conical shell under thermal environment", *P. I. Mech. Eng. C-J. Mec*., **234**(3), 770-783. https://doi.org/10.1177/0954406219886325.

Mohamed, N., Mohamed, S.A. and Eltaher, M.A. (2021), "Buckling and post-buckling behaviors of higher order carbon nanotubes using energy-equivalent model", *Eng. with Comput*., **37**(4), 2823-2836. https://doi.org/10.1007/s00366-020-00976-2.

Mohamed, N., Eltaher, M.A., Mohamed, S.A. and Seddek, L.F. (2019), "Energy equivalent model in analysis of postbuckling of imperfect carbon nanotubes resting on nonlinear elastic foundation", *Struct. Eng. Mech*., **70**(6), 737-750. https://doi.org/10.12989/sem.2019.70.6.737.

Melaibari, A., Mohamed, S.A., Assie, A.E., Shanab, R.A. and Eltaher, M.A. (2023), "Static response of 2D FG porous plates resting on elastic foundation using midplane and neutral surfaces with movable constraints", *Mathematics*, **10**(24), 4784. https://doi.org/10.3390/math10244784.

Nguyen, P.D., Quang, V.D., Anh, V.T. and Duc, N.D. (2019), "Nonlinear vibration of carbon nanotube reinforced composite truncated conical shells in thermal environment", *Int. J. Struct. Stab. Dy*., **19**(12), 1950158. https://doi.org/10.1142/S021945541950158X.

Rout, M. and Karmakar, A. (2019), "Free vibration of rotating pretwisted CNTs-reinforced shallow shells in thermal environment", *Mech. Adv. Mater. Struc*., **26**(21), 1808-1820. https://doi.org/ 10.1080/15376494.2018.1452317.

Rout, M., Pani, S. and Mahakud, J. (2021), "A solution to free vibration of rotating pretwisted functionally graded conical shell under nonlinear thermal environments", *J. Braz. Soc. Mech. Sci*., **43**(6), 285. https://doi.org/ 10.1007/s40430-021-02995-6.

Safarpour, H., Hajilak, Z.E. and Habibi, M. (2019), "A size-dependent exact theory for thermal buckling, free and forced vibration analysis of temperature dependent FG multilayer GPLRC composite nanostructures restring on elastic foundation", *Int. J. Mech. Mater. Des*., **15**(3), 569-583. https://doi.org/ 10.1007/s10999-018-9431-8.

Shakouri, M. (2019), "Free vibration analysis of functionally graded rotating conical shells in thermal environment", *Compos. Part. B-Eng*., **163**, 574-584. https://doi.org/10.1016/j.compositesb.2019.01.007.

Shi, J.W. and Teng, X.X. (2021), "Numerical forced vibration analysis of compositionally gradient porous cylindrical micro-shells under moving load and thermal environment", *Steel. Compos. Struct*., **40**(6), 893-902. https://doi.org/10.12989/scs.2021.40.6.893.

She, G.L. (2021), "Guided wave propagation of porous functionally graded plates: The effect of thermal loadings", *J. Therm. Stresses*, **44**(10), 1289-1305. https://doi.org/10.1080/01495739.2021.1974323.

She, G.L., Liu, H.B. and Karami, B. (2021), "Resonance analysis of composite curved microbeams reinforced with graphene nanoplatelets", *Thin Wall. Struct*., **160**, 107407. https://doi.org/10.1016/j.tws.2020.107407.

She, G.L. and Ding, H.X. (2023), "Nonlinear primary resonance analysis of initially stressed graphene platelet reinforced metal foams doubly curved shells with geometric imperfection", *Acta Mech. Sin*., **39**, 522392. https://doi.org/10.1007/s10409-022-22392-x

She, G.L., Ding, H.X. and Zhang, Y.W. (2022), "Wave propagation in a FG circular plate via the physical neutral surface concept", *Struct. Eng. Mech*., **82**(2), 225-232. https://doi.org/10.12989/sem.2022.82.2.225.

She, G.L. and Li, Y.P. (2022), "Wave propagation in an FG circular plate in thermal environment", *Geomech. Eng*., **31**(6), 615-622. https://doi.org/10.12989/gae.2022.31.6.615.

Song, J.P. and She, G.L. (2023), "Nonlinear resonance of axially moving GPLRMF plates with different boundary conditions", *Struct. Eng. Sci*., **86**(3), 361-371. https://doi.org/10.12989/sem.2023.86.3.361.

Tu, T.M., Thai, D.K., Hoan, P.V. and Hoa, L.K. (2021), "Nonlinear behavior of FG porous cylindrical sandwich shells reinforced by spiral stiffeners under torsional load including thermal effect", *Mech. Adv. Mater. Struc*. https://doi.org/10.1080/15376494.2021.1967530.

Wang, X.J., Mao, H.T., Wang, F., Gu, Y. and Mohammadi, R. (2021), "Size-dependent analysis of the spherical nanoshells subjected to a moving harmonic load in hygro-thermo environment", *Wave. Random. Complex*, https://doi.org/10.1080/17455030.2021.2017512.

Wang, Y. and Wu, D. (2017), "Free vibration of functionally graded porous cylindrical shell using a sinusoidal shear deformation theory", *Aerosp. Sci. Technol*., **66**, 83-91. https://doi.org/10.1016/j.ast.2017.03.003.

Wang. Y.Q., Ye. C. and Zu. J.W. (2019) "Nonlinear vibration of metal foam cylindrical shells reinforced with graphene platelets", *Aerosp. Sci. Technol*., **85**, 359-370. https://doi.org/10.1016/j.ast.2018.12.022.

Wang, Y. and Zhang, W. (2022), "On the thermal buckling and post-buckling responses oftemperature-dependent graphene platelets reinforced porous nanocomposite beams", *Compos. Struct*., **296**, 115880. https://doi.org/10.1016/j.compstruct.2022.115880.

Wu, F. and She, G.L. (2023), "Wave propagation in double nano-beams in thermal environments using the Reddy's high-order shear deformation theory", *Adv. Nano Res*., **14**(6), 495-506. https://doi.org/10.12989/anr.2023.14.6.495.

Xu, J.Q. and She, G.L. (2022), "Thermal post-buckling analysis of porous functionally graded pipes with initial geometric imperfection", *Geomech. Eng*., **31**(3), 329-337. https://doi.org/10.12989/gae.2022.31.3.329.

Xu, J.Q. and She, G.L. (2023), "Thermal post-buckling of graphene platelet reinforced metal foams doubly curved shells with geometric imperfection", *Struct. Eng. Mech*., **87**(1), 85-94. https://doi.org/10.12989/sem.2023.87.1.085.

Xu, J.Q., She, G.L., Li. Y.P. and Gan, L.L. (2023), "Nonlinear resonances of nonlocal strain gradient nanoplates made of functionally graded materials considering geometric imperfection", *Steel Compos. Struct*., **47**(6), 795-811. https://doi.org/10.12989/scs.2023.47.6.795.

Zhang, Y.W., Ding, H.X. and She, G.L. (2022), "Snap-buckling and resonance of functionally graded graphene reinforced composites curved beams resting on elastic foundations in thermal environment", *J. Therm. Stresses*, **45**(12), 1029-1042. https://doi.org/10.1080/01495739.2022.2125137.

Zhang, Y.W., Ding, H.X. and She, G.L. (2023a), "Wave propagation in spherical and cylindrical panels reinforced with carbon nanotubes", *Steel Compos. Struct*., **46**(1), 133-141. https://doi.org/10.12989/scs.2023.46.1.133.

Zhang, Y.W., She, G.L. and Ding, H.X. (2023b), "Nonlinear resonance of graphene platelets reinforced metal foams plates under axial motion with geometric imperfections", *Eur. J. Mech. A-Solid*., **98**, 104887. https://doi.org/10.1016/j.euromechsol.2022.104887.

Zhang, Y.W., She, G.L., Gan, L.L. and Li, Y.P. (2023c), "Thermal post-buckling behavior of GPLRMF cylindrical shells with initial geometrical imperfection", *Geomech. Eng*., **32**(6), 615625. https://doi.org/10.12989/gae.2023.32.6.615

Zhang, Y.W., Ding, H.X., She, G.L. and Tounsi, A. (2023d), "Wave propagation of CNTRC beams resting on elastic foundation based on various higher-order beam theories", *Geomech. Eng*., **33**(4), 381-391. https://doi.org/10.12989/gae.2023.33.4.381.

Zhang, Y.W. and She, G.L. (2022), "Wave propagation and vibration of FG pipes conveying hot fluid", *Steel. Compos, Struct.*, **42**(3) 397-405. https://doi.org/10.12989/scs.2022.42.3.397.

Zhang, Y.W. and She, G.L. (2023a), "Nonlinear low-velocity impact response of graphene platelet-reinforced metal foam cylindrical shells under axial motion with geometrical imperfection", *Nonlinear Dynamics*, **111**(7), 6317-6334. https://doi.org/10.1007/s11071-022-08186-9.

Zhang, Y.W. and She, G.L. (2023b), "Nonlinear primary resonance of axially moving functionally graded cylindrical shells in thermal environment", *Mech. Adv. Mater. Struc*., https://doi.org/10.1080/15376494.2023.2180556

Zhang, Y.Y., Wang, X.Y., Zhang, X., Shen, H.M., and She, G.L. (2021), "On snap-buckling of FG-CNTRC curved nanobeams considering surface effects", *Steel Compos. Struct*., **38**(3), 293-304. https://doi.org/10.12989/scs.2021.38.3.293.

Zhao, J.L., Chen, X., She, G.L., Jing, Y., Bai, R.Q., Yi, J., Pu, H.Y. and Luo, J. (2022a), "Vibration characteristics of functionally graded carbon nanotube-reinforced composite double-beams in thermal environments", *Steel. Compos. Struct*., **43**(6), 797-808. https://doi.org/10.12989/scs.2022.43.6.797.

Zhao, J.L., She, G.L., Wu, F., Yuan, S.J., Bai, R.Q., Pu, H.Y., Wang, S.L. and Luo, J. (2022b), "Guided waves of porous FG nanoplates with four edges clamped", *Adv. Nano. Res.*, **13**(5), 465-474. https://doi.org/10.12989/anr.2022.13.5.465.

Zu, X.D., Gao, Z.J., Zhao, J., Wang, Q.S. and Li, H. (2022), "Vibration suppression performance of FRP spherical-cylindrical shells with porous graphene platelet coating in a thermal environment", *Int. J. Struct. Stab. Dy*., **22**(8), 2250081. https://doi.org/10.1142/S021945542250081X.

CC

Appendix

$$\left[-\frac{\pi^2\left(A_{66}a^2n^2+A_{11}b^2m^2\right)}{4ab}\right]\mathbf{U(t)}+\left[-\frac{mn\pi^2\left(A_{12}+A_{66}\right)}{4}\right]\mathbf{V(t)}+\left[-\frac{\pi bm\left(A_{12}R_x+A_{11}R_y\right)}{4R_xR_y}\right]\mathbf{W(t)}+\left[-\frac{\pi^2\left(B_{11}b^2m^2+B_{66}a^2n^2-E_{11}b^2c_1m^2-E_{66}a^2c_1n^2\right)}{4ab}\right]\mathbf{\Phi_x(t)}+\left[-\frac{mn\pi^2\left(B_{12}+B_{66}-E_{12}c_1-E_{66}c_1\right)}{4}\right]\mathbf{\Phi_y(t)}=0,$$

$$\left[-\frac{\pi an\left(A_{22}R_x+A_{12}R_y\right)}{4R_xR_y}\right]\mathbf{W(t)}-\left[\frac{mn\pi^2\left(A_{12}+A_{66}\right)}{4}\right]\mathbf{U(t)}+\left[-\frac{\pi^2\left(A_{22}a^2n^2+A_{66}b^2m^2\right)}{4ab}\right]\mathbf{V(t)}+\left[-\frac{mn\pi^2\left(B_{12}+B_{66}-E_{12}c_1-E_{66}c_1\right)}{4}\right]\mathbf{\Phi_x(t)}-\left[\frac{\pi^2\left(B_{22}a^2n^2+B_{66}b^2m^2-E_{22}a^2c_1n^2-E_{66}b^2c_1m^2\right)}{4ab}\right]\mathbf{\Phi_y(t)}=0,$$

$$\left[\frac{\pi m\left(A_{12}R_xa^2b^2+A_{11}R_ya^2b^2+E_{11}R_xR_yb^2c_1m^2\pi^2\right)}{4R_xR_ya^2b}\right]\mathbf{U(t)}+\left[\frac{\pi m\left(E_{12}R_xR_ya^2c_1n^2\pi^2+2E_{66}R_xR_ya^2c_1n^2\pi^2\right)}{4R_xR_ya^2b}\right]\mathbf{U(t)}+\left[\frac{\pi n\left(A_{22}R_xa^2b^2+A_{12}R_ya^2b^2+E_{12}R_xR_yb^2c_1m^2\pi^2\right)}{4R_xR_yab^2}\right]\mathbf{V(t)}+\left[\frac{\pi n\left(E_{22}R_xR_ya^2c_1n^2\pi^2+2E_{66}R_xR_yb^2c_1m^2\pi^2\right)}{4R_xR_yab^2}\right]\mathbf{V(t)}+\left[\frac{8A_{11}bmw_1}{9R_xan}-\frac{A_{22}ab}{4R_y^2}-\frac{A_{55}bm^2\pi^2}{4a}-\frac{A_{44}an^2\pi^2}{4b}\right]\mathbf{W(t)}+\left[\frac{8A_{12}anw_1}{9R_xbm}-\frac{\mathrm{Phbm}^2\pi^2}{4a}-\frac{A_{12}ab}{2R_xR_y}-\frac{F_{55}bc_2{}^2m^2\pi^2}{4a}\right]\mathbf{W(t)}+\left[\frac{F_{44}ac_2{}^2n^2\pi^2}{4b}+\frac{D_{55}bc_2m^2\pi^2}{2a}+\frac{D_{44}ac_2n^2\pi^2}{2b}+\frac{A_{11}ab}{4R_x^2}\right]\mathbf{W(t)}+\left[\frac{8A_{12}bmw_1}{9R_yan}+\frac{8A_{22}anw_1}{9R_ybm}+\frac{E_{11}bc_1m^2\pi^2}{4R_xa}+\frac{E_{12}ac_1n^2\pi^2}{4R_xb}\right]\mathbf{W(t)}+\left[\frac{E_{12}ac_1n^2\pi^2}{4R_yb}+\frac{16E_{22}ac_1n^3w_1\pi^2}{9b^3m}+\frac{E_{22}ac_1n^2\pi^2}{4R_yb}\right]\mathbf{W(t)}+\left[\frac{16E_{66}c_1mnw_1\pi^2}{9ab}+\frac{16E_{11}bc_1m^3w_1\pi^2}{9a^3n}\right]\mathbf{W(t)}+\left[\frac{an\pi^2+bm\pi^2}{4a}N^T-\frac{16E_{12}c_1mnw_1\pi^2}{9ab}\right]\mathbf{W(t)}+\left[\frac{20A_{11}bm}{9R_xan}+\frac{20A_{12}an}{9R_xbm}+\frac{20A_{12}bm}{9R_yan}+\frac{20A_{22}an}{9R_ybm}\right]\mathbf{W^2(t)}+\left[\frac{8E_{11}bc_1m^3\pi^2}{9a^3n}+\frac{8E_{22}ac_1n^3\pi^2}{9b^3m}-\frac{8E_{12}c_1mn\pi^2}{9ab}\right]\mathbf{W^2(t)}-\left[\frac{w_1\pi^2\left(48A_{22}a^4mn^5\pi^2+48A_{11}b^4m^5n\pi^2\right)}{1024a^3b^3mn}\right]\mathbf{W^2(t)}-\left[\frac{w_1\pi^2\left(96A_{12}a^2b^2m^3n^3\pi^2-64A_{66}a^2b^2m^3n^3\pi^2\right)}{1024a^3b^3mn}\right]\mathbf{W^2(t)}-\left[\frac{\pi^2\left(48A_{22}a^4mn^5\pi^2+48A_{11}b^4m^5n\pi^2\right)}{2048a^3b^3mn}\right]\mathbf{W^3(t)}-\left[\frac{\pi^2\left(96A_{12}a^2b^2m^3n^3\pi^2-64A_{66}a^2b^2m^3n^3\pi^2\right)}{2048a^3b^3mn}\right]\mathbf{W^3(t)}-\left[\frac{\pi^2\left(96A_{12}a^2b^2m^3n^3\pi^2-64A_{66}a^2b^2m^3n^3\pi^2\right)}{2048a^3b^3mn}\right]\mathbf{W^3(t)}+\left[\frac{H_{11}bc_1{}^2m^3\pi^3}{4a^2}-\frac{\pi D_{55}bc_2m}{2}-\frac{\pi B_{11}bm}{4R_x}-\frac{\pi B_{12}bm}{4R_y}\right]\mathbf{\Phi_x(t)}+\left[-\frac{\pi F_{55}bc_2{}^2m}{4}-\frac{\pi A_{55}bm}{4}-\frac{H_{12}c_1{}^2mn^2\pi^3}{4b}\right]\mathbf{\Phi_x(t)}+\left[-\frac{H_{66}c_1{}^2mn^2\pi^3}{2b}+\frac{F_{11}bc_1m^3\pi^3}{4a^2}+\frac{F_{12}c_1mn^2\pi^3}{4b}\right]\mathbf{\Phi_x(t)}+\left[\frac{F_{66}c_1mn^2\pi^3}{2b}+\frac{\pi E_{11}bc_1m}{4R_x}+\frac{\pi E_{12}bc_1m}{4R_y}\right]\mathbf{\Phi_x(t)}+\Pi=0$$

$$\left[-\frac{\pi^2\left(B_{11}b^2m^2+B_{66}a^2n^2-E_{11}b^2c_1m^2-E_{66}a^2c_1n^2\right)}{4ab}\right]\mathbf{U(t)}+\left[-\frac{mn\pi^2\left(B_{12}+B_{66}-E_{12}c_1-E_{66}c_1\right)}{4}\right]\mathbf{V(t)}+\left[\frac{8\pi B_{12}nw_1}{9b}-\frac{8\pi B_{66}nw_1}{9b}-\frac{4\pi E_{12}c_1nw_1}{9b}+\frac{8\pi E_{66}c_1nw_1}{9b}\right]\mathbf{W(t)}-\left[\frac{\pi bm\left(-F_{55}R_xR_yc_2{}^2+B_{12}R_x+B_{11}R_y+A_{55}R_xR_y\right)}{4R_xR_y}\right]\mathbf{W(t)}-\left[\frac{\pi bm\left(-E_{12}R_xc_1-E_{11}R_yc_1\right)}{4R_xR_y}-\frac{16\pi B_{11}bm^2w_1}{9a^2n}\right]\mathbf{W(t)}+\frac{16\pi E_{11}bc_1m^2w_1}{9a^2n}\mathbf{W(t)}-\left[\frac{4\pi\left(2B_{11}b^2m^2-B_{12}a^2n^2\right)}{9a^2bn}\right]\mathbf{W^2(t)}+\left[\frac{4\pi\left(B_{66}a^2n^2-2E_{11}b^2c_1m^2+E_{12}a^2c_1n^2-E_{66}a^2c_1n^2\right)}{9a^2bn}\right]\mathbf{W^2(t)}-\frac{\left(-F_{55}a^2b^2c_2{}^2+A_{55}a^2b^2+H_{66}\pi^2a^2c_1{}^2n^2\right)}{4ab}\mathbf{\Phi_x(t)}-\frac{\left(-2F_{66}\pi^2a^2c_1n^2+D_{66}\pi^2a^2n^2+H_{11}\pi^2b^2c_1{}^2m^2\right)}{4ab}\mathbf{\Phi_x(t)}-\frac{\left(-2F_{11}\pi^2b^2c_1m^2+D_{11}\pi^2b^2m^2\right)}{4ab}\mathbf{\Phi_x(t)}-\frac{mn\pi^2\left(D_{12}\right)}{4}\mathbf{\Phi_y(t)}-\frac{mn\pi^2\left(D_{66}-2F_{12}c_1-2F_{66}c_1+H_{12}c_1{}^2+H_{66}c_1{}^2\right)}{4}\mathbf{\Phi_y(t)}=0,$$

$$\left[-\frac{mn\pi^2\left(B_{12}+B_{66}-E_{12}c_1-E_{66}c_1\right)}{4}\right]\mathbf{U(t)}-\left[\frac{\pi^2\left(B_{22}a^2n^2+B_{66}b^2m^2-E_{22}a^2c_1n^2\right)}{4ab}\right]\mathbf{V(t)}+E_{66}b^2c_1m^2\mathbf{V(t)}+\left[\frac{8\pi w_1\left(B_{12}b^2m^2-2B_{22}a^2n^2\right)}{9ab^2m}\right]\mathbf{W(t)}+\left[\frac{8\pi w_1\left(-B_{66}b^2m^2-E_{12}b^2c_1m^2+2E_{22}a^2c_1n^2\right)}{9ab^2m}\right]\mathbf{W(t)}+\frac{8\pi w_1\left(E_{66}b^2c_1m^2\right)}{9ab^2m}\mathbf{W(t)}-\left[\frac{\pi an\left(-F_{44}R_xR_yc_2{}^2\right)}{4R_xR_y}\right]\mathbf{W(t)}-\left[\frac{\pi an\left(B_{22}R_x+B_{12}R_y+A_{44}R_xR_y-E_{22}R_xc_1\right)}{4R_xR_y}\right]\mathbf{W(t)}+\frac{\pi an\left(E_{12}R_yc_1\right)}{4R_xR_y}\mathbf{W(t)}+\left[\frac{4\pi\left(B_{12}b^2m^2\right)}{9ab^2m}\right]\mathbf{W^2(t)}+\left[\frac{4\pi\left(-2B_{22}a^2n^2-B_{66}b^2m^2-E_{12}b^2c_1m^2\right)}{9ab^2m}\right]\mathbf{W^2(t)}+\left[\frac{4\pi\left(2E_{22}a^2c_1n^2+E_{66}b^2c_1m^2\right)}{9ab^2m}\right]\mathbf{W^2(t)}+\Gamma=0$$

In which

$$\Pi=\left[\frac{H_{22}ac_1{}^2n^3\pi^3}{4b^2}-\frac{\pi D_{44}ac_2n}{2}-\frac{\pi B_{12}an}{4R_x}-\frac{\pi B_{22}an}{4R_y}\right]\mathbf{\Phi_y(t)}+\left[\frac{F_{22}ac_1n^3\pi^3}{4b^2}+\frac{F_{12}c_1m^2n\pi^3}{4a}+\frac{F_{66}c_1m^2n\pi^3}{2a}\right]\mathbf{\Phi_y(t)}+\left[\frac{\pi E_{22}ac_1n}{4R_y}-\frac{H_{66}c_1{}^2m^2n\pi^3}{2a}+\frac{\pi E_{12}ac_1n}{4R_x}\right]\mathbf{\Phi_y(t)}+\left[-\frac{\pi F_{44}ac_2{}^2n}{4}-\frac{\pi A_{44}an}{4}-\frac{H_{12}c_1{}^2m^2n\pi^3}{4a}\right]\mathbf{\Phi_y(t)}+\left[\frac{16\pi A_{12}n}{9b}+\frac{8\pi A_{66}n}{9b}+\frac{16\pi A_{11}bm^2}{9a^2n}\right]\mathbf{U(t)W(t)}+\left[\frac{16\pi A_{12}m}{9a}+\frac{8\pi A_{66}m}{9a}+\frac{16\pi A_{22}an^2}{9b^2m}\right]\mathbf{V(t)W(t)}+\left[\frac{16\pi B_{12}n}{9b}+\frac{8\pi B_{66}n}{9b}-\frac{16\pi E_{12}c_1n}{9b}\right]\mathbf{\Phi_x(t)W(t)}+\left[\frac{16\pi B_{11}bm^2}{9a^2n}-\frac{8\pi E_{66}c_1n}{9b}-\frac{16\pi E_{11}bc_1m^2}{9a^2n}\right]\mathbf{\Phi_x(t)W(t)}+\left[\frac{16\pi B_{12}m}{9a}+\frac{8\pi B_{66}m}{9a}-\frac{16\pi E_{12}c_1m}{9a}\right]\mathbf{\Phi_y(t)W(t)}+\left[\frac{16\pi B_{22}an^2}{9b^2m}-\frac{8\pi E_{66}c_1m}{9a}-\frac{16\pi E_{22}ac_1n^2}{9b^2m}\right]\mathbf{\Phi_y(t)W(t)}+q=I_1\frac{\partial^2\mathbf{W(t)}}{\partial t^2},$$

(A1) (A2) (A3) (A4) (A5) (A6)

$$\Gamma = -\left[\frac{mn\pi^2\left(D_{12}+D_{66}-2F_{12}c_1-2F_{66}c_1\right)}{4}\right]\boldsymbol{\Phi}_{\mathbf{x}}(\mathbf{t})$$
$$-\left[\frac{mn\pi^2\left(H_{12}c_1^{\,2}+H_{66}c_1^{\,2}\right)}{4}\right]\boldsymbol{\Phi}_{\mathbf{x}}(\mathbf{t})$$
$$-\frac{\left(-F_{44}a^2b^2c_2^{\,2}+A_{44}a^2b^2+H_{22}\pi^2a^2c_1^{\,2}n^2\right)}{4ab}\boldsymbol{\Phi}_{\mathbf{y}}(\mathbf{t}) \qquad \text{(A7)}$$
$$-\frac{\left(-2F_{22}\pi^2a^2c_1n^2+H_{66}\pi^2b^2c_1^{\,2}m^2\right)}{4ab}\boldsymbol{\Phi}_{\mathbf{y}}(\mathbf{t})$$
$$-\frac{\left(D_{22}\pi^2a^2n^2-2F_{66}\pi^2b^2c_1m^2+D_{66}\pi^2b^2m^2\right)}{4ab}\boldsymbol{\Phi}_{\mathbf{y}}(\mathbf{t})$$